International Journal of Advances in Scientific Research and Engineering (ijasre)

E-ISSN : 2454-8006

DOI: 10.31695/IJASRE.2022.8.10.1

Volume 8, Issue 10
October - 2022

IRS-Assisted OAM-MIMO Communication with Partial Arc Sampling Receiving (PASR) Scheme

Ndagijimana Cyprien[1], Yang Wang[1*], Hailay Teklehaimanot Belay[2], Hungurimana Olivier[3]

Research Scholar[1,2,3], Professor[1*]

[1,2]School of Communication and Information Engineering

Chongqing University of Posts and Telecommunications

Chongqing, China

[3]School of computational and Communication Sciences and Engineering

Nelson Mandela African Institution of Science and Technology

Arusha, Tanzania

ABSTRACT

Orbital Angular Momentum-based Multiple Inputs Multiple Outputs (OAM-MIMO) Communication has recently been explored in wireless communication to provide an alternative way of multiplexing different orthogonal OAM modes over a common medium and significantly improve reliability, capacity, and energy efficiency. Although the near-field applications of radio vortex have been successfully verified in a near-field line-of-sight scenario, perfect antenna misalignment should be required to maintain orthogonality, which is difficult to be satisfied in a multipath environment consisting of many non-line-of-sight (NLOS) paths and LOS path. In addition, beam spread and divergence reduce the transmission distance accompanied by large performance degradation, thus requiring a large aperture size receiving for efficient detection of OAM modes. This paper studies the communication performance of OAM-MIMO with the PASR (Partial Aperture Sampling Receiving) scheme by deploying an intelligent reflective surface (IRS) of a large number of reconfigurable passive elements to achieve an intelligent wireless propagation environment through software-controlled reflection and address the above issues and limitations under the Perfect Channel State Information (CSI). We analyze the concepts of PASR and OAM mode selection by preserving orthogonality according to the required aperture scale, and the influence of the Rayleigh and Rician channels on the system performance of IRS-Assisted OAM-MIMO Communication with the PASR scheme in a multipath environment. The simulation results show that the channel capacity for IRS-assisted OAM-MIMO Communication with the PASR scheme is greatly improved compared with IRS-assisted OAM-MIMO Communication, which can meet the performance requirements, and provide insights into the angular aperture needed for efficient (de)-multiplex OAM modes, and performance limit over propagation distance.

Keywords: OAM-based MIMO Communication, Intelligent Reflecting Surface, Partial angular aperture receiving scheme.

I. INTRODUCTION

A great demand for high-capacity wireless data communications has grown exponentially each year, while this continued growth has been exacerbated by the broadband cellular services originating from plenty of wireless devices. As an effective countermeasure, research efforts are heavily focused on feasible and innovative communication technologies with the increasing need for network capacity [1]. Under these concerns, key enabler technologies such as Ultra-dense networks [2], Massive MIMO (Multiple Input Multiple Output) [3], mmWave communications [4], and OFDM (Orthogonal Frequency Division Multiplexing) [5] have been developed to fulfill the network capacity requirements. Even considering these technologies, it is not easy to enhance the spectrum efficiency without increasing additional resources, and they face major practical limitations. From a power consumption perspective, they consume large amounts of power and incur high hardware/spectrum provisioning costs, which are critical points for practical deployment [6]. Also, they face difficulties to provide a quality of service guarantee in harsh propagation environments due to the lack of control over the wireless channels [7].

In addition, high path attenuation, especially at mmWave frequencies, limits the network coverage and leads to blockages, multipath propagation leads to fading, while anomalous refraction/reflections from surrounding objects lead to uncontrollable interference [8]. In view of the above issues and limitations, the next 6G wireless networks have been proposed, which are expected to achieve smarter and superior performance than 5G. As the enabling technology of 6G, OAM-based wireless communication has gained more prominence as an innovative technique to multiplex a variety of orthogonal OAM modes on an identical frequency channel to attain high spectral efficiency, energy efficiency [9], and reliability [10]. It is reported in [11], [12] that OAM multiplexing offers a new degree of freedom, that is, Mode Division Multiplexing (MDM). With this approach, OAM-based wireless communication is able to increase capacity without using additional traditional resources. It is inspired that combining Orbital Angular Momentum (OAM) with multiple input multiple outputs (MIMO) results in a high capacity gain, and reduces the spread of OAM beams upon increasing multiplexing order [13]. Due to its properties of generating multiple vortex beams simultaneously, Uniform Circular Array (UCA) has been the pioneering approach to high-capacity transmission as proposed in [14].

Practically, a multipath environment consisting of Non-Line-of-Sight (NLOS) and LOS paths has a significant impact on the system performance for OAM-based wireless communication [15]. Various convergence and long-distance transmission schemes for OAM beams have been proposed as potential solutions to deal with divergence problems [16], [17]. The innovative partial aperture sampling receiving scheme called PASR was introduced as an effective space-saving method for receiving and de-multiplexing OAM modes in OAM-based wireless communication [18], [19]. Furthermore, in [20], the authors analyzed the stability of the OAM communication system with a partial angular aperture receiving (PAAR) scheme under the atmospheric turbulence environment. In [21], [22] it was shown that Intelligent Reflecting Surface (IRS) can support orbital angular momentum based Multiple Inputs Multiple Outputs (OAM-MIMO) to improve the system performance of OAM-based wireless communication. Even if the feasibility of OAM-based wireless communication has been successfully verified, antenna misalignment; beam spreading and divergence problems reduce the transmission distance accompanied by large performance degradation [23]. In addition, controlling the propagation of radio vortex waves in a multipath environment is still the biggest challenge, thus leaving the ultimate barrier to achieving high-capacity and ultra-reliable wireless communications.

2. OBJECTIVE OF RESEARCH

The objective of this paper is to improve the system capacity of OAM-based wireless communication by considering the impact of the IRS as well as the PASR scheme on the system performance under the perfect channel state information (CSI). Theoretically, we analyze the concepts of PASR and OAM mode selection by preserving orthogonality according to the required aperture scale in Section II. Then, a generalized signal model of the IRS-Assisted OAM-MIMO Communication with partial aperture sampling receiving is derived analytically in Section III. Based on that, the theoretical analysis of the proposed system is presented and the numerical results are taken further to evaluate its performance compared to the system without PASR in section IV, and conclusions are drawn in section VI.

2.1 Concept of The Pasr Scheme

The divergence of OAM vortex waves becomes more severe when propagating over a long distance because of the beams spreading, resulting in large performance degradation [22]. This requires a large receiving aperture for effective reception of the vortex beams, but this could be difficult to achieve. To solve this problem, several detection methods have been proposed, and the PASR scheme has been considered to use partial wave-front information to detect and demultiplex different OAM modes. The PASR scheme combines the partial angular receiving aperture method for OAM de-multiplexing (Fig. 1, (a)), and a sampling receiving scheme (Fig. 1, (b)). The perimeter of the receiving aperture for scanning is in the receiving plane. The receiving plane is perpendicular to the beam axis and the center of the perimeter of the receiving aperture is on the z-axis.

In particular, the M antennas at the receiver are evenly distributed along an arc which is $1/\mu$ of a circle having a circular perimeter with a radius of R_r. Then the two adjacent antennas are separated by an angular difference of $2\pi/M\mu$, and the PASR really occupies an angular aperture of $2\pi(M-1)/M\mu$. To analyze the orthogonality between modes, we consider two periodic functions of different OAM modes (i.e. l_1 and l_2) written as:

$$E_1 = A_1(\rho, z)e^{-jl_1\vartheta} \quad (1)$$

$$E_2 = A_2(\rho, z)e^{-jl_2\vartheta} \quad (2)$$

where $A_1(\rho,z)$ and $A_2(\rho,z)$ represent the path loss with respect to radial position ρ and propagation distance z. It is worth noting that the orthogonality will be maintained when:

DOI: 10.31695/IJASRE.2022.8.10.1

$$\sum_{m=1}^{M-1} E_1(\frac{2\pi m}{\mu M}) E_2^*(\frac{2\pi m}{\mu M}) = A_1 A_2^* \sum_{m=0}^{M-1} e^{-j\frac{2\pi m}{M}\frac{l_1 - l_2}{\mu}} = A_1 A_2^* \sum_{m=0}^{M-1} e^{-j\frac{2\pi m}{M}k} = 0 \quad (3)$$

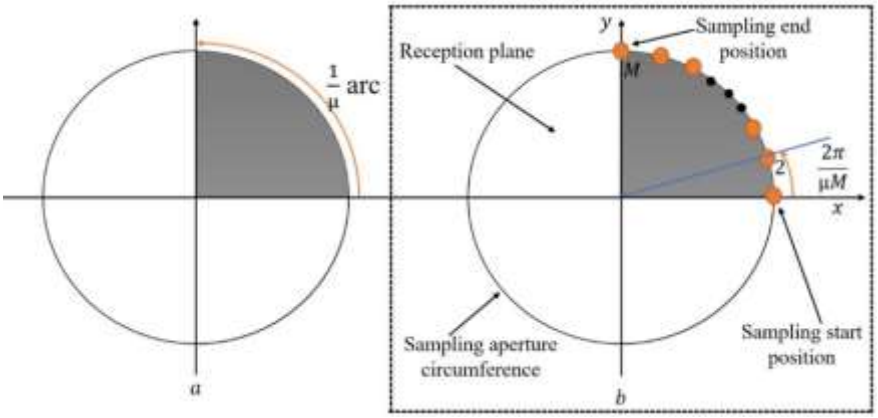

Figure 1. The geometry of the PASR scheme with *M* antennas distributed along a circular arc.

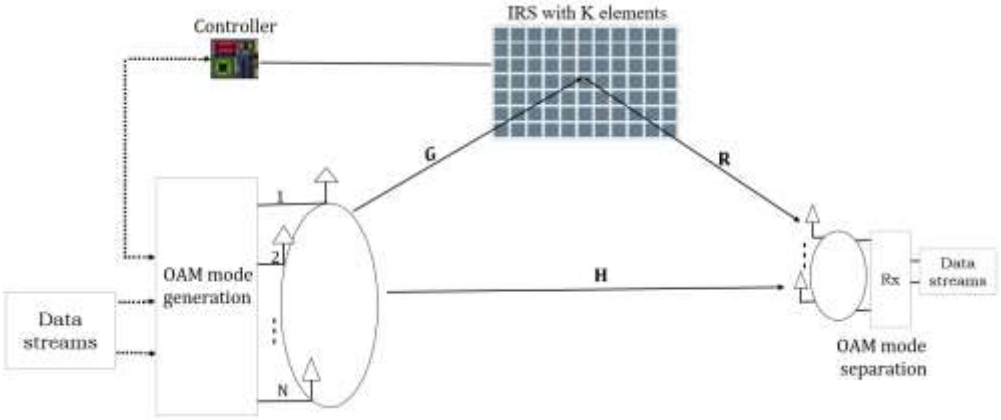

Figure 2 Intelligent Reflecting Surface assisted OAM-MIMO system with PASR scheme.

3. IRS-ASSISTED OAM-MIMO WIRELESS COMMUNICATION WITH PASR

The system structure of an IRS-assisted OAM-MIMO communication based on the PASR scheme is described in Fig.2. As shown, the UCA-based transmitter consists of *N* antenna elements that simultaneously generate N OAM modes with the inverse discrete Fourier transform (IDFT) matrix and are received by *M* antenna elements at UCA based receiver with PASR scheme. In practice, perfect alignment between transmit and receive UCAs may be difficult to realize. In our consideration, the *K* elements of the IRS are located in the line-of-sight (LOS) of the transmitter; and are configured to reflect and guide the signals to the receiver. By appropriately controlling the phase shifts and amplitude coefficients of the IRS elements, the vortex signals can be advantageously manipulated. We consider that the IRS of *K* reflecting elements, located in the line-of-sight (LOS) of the transmitter, is configured to reflect and direct the signals toward the receiver. We denote $\boldsymbol{G} \in \mathbb{C}^{K \times N}$, $\boldsymbol{R} \in \mathbb{C}^{M \times K}$ and $\boldsymbol{H} \in \mathbb{C}^{M \times N}$ the channel matrices between transmitter-to-IRS, IRS-to-receiver, and transmitter-to-receiver, respectively. In other words, each element of the IRS receives the superimposed multipath signals from the transmitter and then scatters the combined signal with optimal amplitude and phase shift as if it came from a single-point source. Note that the signals reflected more than once by the IRS are also ignored due to the high path attenuation [24].

3.1 Signal Model

We define the expression for the transmitted vortex signal on the transmitter side as follows:

$$x_n = \sum_{l \in L} \frac{1}{\sqrt{N}} p_l s_l e^{j\psi_n l} \quad (4)$$

where p_l and s_l represent the power and symbol of the l^{th} OAM-mode, ψ_n is the azimuth angle, defined as the angular position corresponding to the nth antenna element on the transmit UCA. Therefore, the angular position ψ_n with the PASR is given by

DOI: 10.31695/IJASRE.2022.8.10.1

$$\psi_n = 2\pi\left(\frac{(n-1)}{\mu N}\right)+\phi \tag{5}$$

Without loss generality, we assume that the first antenna element is placed at zero radians, while the second antenna element is placed at ϕ. By changing the value of ϕ, we can obtain all possible relative rotations between two array element UCAs. The source transmits the OAM vector $\boldsymbol{x}$ generated by the DFT matrix as expressed below:

$$\boldsymbol{X} = \boldsymbol{PsF}_T^H \tag{6}$$

where $x=\left[x_0, x_1, ..., x_{L-1}\right]^T$, $P = diag\left\{p_0, p_1, ..., p_{L-1}\right\}$ is the diagonal matrix with entry p_l corresponding to the l^{th} OAM-mode. The vector $s=\left[s_0, s_1, ..., s_{L-1}\right]^T$ and $\mathrm{E}\left\{s^H s\right\}=1$ where {.} denotes the expectation operation while $(.)^H$ represents the conjugate transpose operation. In addition, the OAM generation matrix $\boldsymbol{F}_T=\left[f_{n,l}\right]_{N\times L}$ is expressed as:

$$\boldsymbol{F}_T = \begin{pmatrix} e^{jl_1\psi_n(1)} & e^{jl_2\psi_n(1)} & \cdots & e^{jl_L\psi_n(1)} \\ e^{jl_1\psi_n(2)} & e^{jl_2\psi_n(2)} & \cdots & e^{jl_L\psi_n(2)} \\ \vdots & \vdots & \ddots & \vdots \\ e^{jl_1\psi_n(N)} & e^{jl_2\psi_n(N)} & \cdots & e^{jl_L\psi_n(N)} \end{pmatrix} \tag{7}$$

At the receiver, by ignoring the secondary or multiple reflections from the IRS, the received signal is then expressed as follows:

$$\boldsymbol{y} = \left(\boldsymbol{H}+\boldsymbol{G\Theta R}\right)\boldsymbol{x}+\boldsymbol{z} = \left(\boldsymbol{H}+\boldsymbol{G\Theta R}\right)\boldsymbol{PsF}_T^H+\boldsymbol{z} \tag{8}$$

where $z=\left[z_0, z_1, ..., z_{L-1}\right]^T$ is the additive Gaussian noise with variance σ^2 and $\mathrm{H}=\boldsymbol{H}+\boldsymbol{G\Theta R}$ is the cascaded channel matrix of the IRS assisted system and the reflection properties of the k^{th} element of IRS are fully represented by the diagonal matrix $\Theta = diag(\beta_1 e^{j\theta_1}, ..., \beta_k e^{j\theta_k}, ..., \beta_K e^{j\theta_K})$ where $\theta_k \in [0, 2\pi]$ and $\beta_k \in [0, 1]$ denote the phase shift and amplitude reflection coefficient introduced by the k^{th} element of the IRS. We assume that β_k is the same for all elements of the IRS. Note that the optimal phase shift variable derived in [25] under the perfect CSI at the IRS. The received vortex signals are firstly pre-detected, so that the transmitted signals can be recovered using the discrete Fourier transform (DFT) while also discarding interference from other signals as follows:

$$\boldsymbol{r} = \boldsymbol{W}_R\left(\boldsymbol{H}+\boldsymbol{G\Theta R}\right)\boldsymbol{PsF}_T^H+\tilde{\boldsymbol{z}} \tag{9}$$

Where $\boldsymbol{W}_R\left(\boldsymbol{H}+\boldsymbol{G\Theta R}\right)\boldsymbol{F}_T^H$ represents the channel matrix for IRS-assisted OAM-MIMO communication system with PASR and $\tilde{\boldsymbol{z}}$ has the same distribution as **z**. Note that the OAM demodulation matrix $\boldsymbol{W}_R=\left[w_{m,l}\right]_{L\times M}$ is expressed as:

$$\boldsymbol{W}_R = \begin{pmatrix} e^{-jl_1\psi_n(1)} & e^{jl_1\psi_n(2)} & \cdots & e^{-jl_1\psi_n(M)} \\ e^{-jl_2\psi_n(1)} & e^{jl_2\psi_n(2)} & \cdots & e^{-jl_2\psi_n(M)} \\ \vdots & \vdots & \ddots & \vdots \\ e^{-jl_L\psi_n(1)} & e^{jl_L\psi_n(2)} & \cdots & e^{-jl_L\psi_n(M)} \end{pmatrix} \tag{10}$$

Note that the effective OAM channel matrix for the IRS-assisted OAM-MIMO communication system with the PASR denoted by $\boldsymbol{H}_{OAM} \in \mathbb{C}^{L\times L}$ can be written as:

$$\boldsymbol{H}_{OAM}^{PASR} = \boldsymbol{W}_R \mathrm{H} \boldsymbol{F}_T^H = \begin{pmatrix} h_{1,1}^{PASR} & h_{1,2}^{PASR} & \cdots & h_{1,L}^{PASR} \\ h_{2,1}^{PASR} & h_{2,2}^{PASR} & \cdots & h_{2,L}^{PASR} \\ \vdots & \vdots & \ddots & \vdots \\ h_{L,1}^{PASR} & h_{L,2}^{PASR} & \cdots & h_{L,L}^{PASR} \end{pmatrix} \tag{11}$$

DOI: 10.31695/IJASRE.2022.8.10.1

Where the i^{th} diagonal element $h_{i,i}^{PASR}$ is OAM channel transmission gain with Eigen mode l_i, and $h_{i,j}^{PASR}$ $(i \neq j)$ indicates the mode migration of the l_i-mode OAM channel to channels of other modes.

3.2 Channel Model

The LoS wireless communication system between transmit and receive UCAs leads to attenuation and phase rotation of the transmitted signal, this effect is modelled in the following expression:

$$h_{m,n} = \eta \frac{\lambda}{4\pi d_{m,n}} \exp\left(-j2\pi \frac{d_{m,n}}{\lambda}\right) \tag{12}$$

where $\lambda/\pi d_{m,n}$ is the free space path loss, λ is the wavelength and η corresponds to all relevant constants such as attenuation and phase rotation of the transmitted signal, $d_{m,n}$ is the distance between the n^{th} transmitting and the m^{th} receiving elements of UCAs and is modeled as:

$$d_{m,n} = \sqrt{R_t^2 + R_r^2 + d^2 - 2R_t R_r \cos\vartheta_{m,n}} \tag{13}$$

where d is the distance between transmit and the receive UCA centers, $\varphi_{m,n} = 2\pi(\frac{\mathrm{m}}{\mathrm{M}} - \frac{\mathrm{n}}{\mathrm{N}})$ denotes the rotation angle between the n^{th} transmitting and the m^{th} receiving elements of UCAs. Since the LoS path between transmitter and IRS and that between IRS and receiver may be blocked, the wireless channel is typically sparsely scattered. We therefore generate the $\boldsymbol{G}$ and $\boldsymbol{R}$ channels using Rician Fading channels modelling as follows:

$$\boldsymbol{G} = \left(\sqrt{\frac{1}{\xi_{TI}}\left(\frac{v}{v+1}\right)}\boldsymbol{G}_{TI}^{LoS} + \sqrt{\frac{1}{\xi_{TI}}\left(\frac{1}{v+1}\right)}\boldsymbol{G}_{TI}^{NLoS}\right) \tag{14}$$

where ξ_{TI} represents the large scale fading effect, ν is the Rician factors, $\boldsymbol{G}_{TI}^{LoS}$ and $\boldsymbol{G}_{TI}^{NLoS}$ denote the *LoS* component and Rayleigh fading component for channel $\boldsymbol{G}$. These components are defined as:

$$\boldsymbol{G}_{TI}^{LoS} = \sqrt{NK}\boldsymbol{a}_{Tx}^{H}\left(\varphi_{Tx},\phi_{Tx}\right)\boldsymbol{b}_{IRS}\left(\varphi_{IRS},\phi_{IRS}\right) \tag{15}$$

and

$$\boldsymbol{G}_{TI}^{NLoS} = \sqrt{\frac{NK}{S}}\sum_{s=1}^{S}\alpha_s \boldsymbol{a}_{Tx}^{H}\left(\varphi_{Tx,s},\phi_{Tx,s}\right)\boldsymbol{b}_{IRS}\left(\varphi_{IRS,s},\phi_{IRS,s}\right) \tag{16}$$

where S is the number of paths, $\varphi_{Tx}(\phi_{Tx})$ and φ_{IRS} (ϕ_{IRS}) are the random azimuth (elevation) angles of departure and arrival (AoD/AoA) associated with the *LOS* component, $\varphi_{Tx,s}(\phi_{Tx,s})$ and $\varphi_{IRS,s}(\phi_{IRS,s})$ are the random azimuth(elevation) angles of departure and arrival (AoD/AoA) associated with the *NLOS* component, and the complex gains α_s is taken by $\alpha_s \sim \mathrm{NC}(0,1)$. Specifically, the IRS-receiver channel $\boldsymbol{R}$ modelled with Rician fading channels is expressed as:

$$\boldsymbol{R} = \left(\sqrt{\frac{1}{\xi_{IR}}\left(\frac{v}{v+1}\right)}\boldsymbol{R}_{IR}^{LoS} + \sqrt{\frac{1}{\xi_{IR}}\left(\frac{1}{v+1}\right)}\boldsymbol{R}_{IR}^{NLoS}\right) \tag{17}$$

where ξ_{IR} represents the large scale fading effect for IRS-to-receiver link, $\boldsymbol{R}_{IR}^{LoS}$ and $\boldsymbol{R}_{IR}^{NLoS}$ denotes the *LoS* and *NLoS* components of channel matrix $\boldsymbol{R}$, which are given by:

$$\boldsymbol{R}_{TI}^{LoS} = \sqrt{KM}\left(\boldsymbol{b}_{IRS}^{H}\left(\varphi_{IRS},\phi_{IRS}\right)\boldsymbol{a}_{Rx}\left(\varphi_{Rx},\phi_{Rx}\right)\right) \tag{18}$$

and

$$\boldsymbol{R}_{IR}^{NLoS} = \sqrt{\frac{KM}{S}}\sum_{s=1}^{S}\alpha_s \boldsymbol{b}_{IRS}^{H}\left(\varphi_{IRS},\phi_{IRS}\right)\boldsymbol{a}_{Rx}\left(\varphi_{Rx,s},\phi_{Rx,s}\right) \tag{19}$$

In the above equation, K and M are the number of antenna elements at the IRS and the receiver, respectively, $\varphi_{Rx,s}(\phi_{Rx,s})$ and $\varphi_{IRS,s}(\phi_{IRS,s})$ represent the random azimuth (elevation) angles of arrival and departure (AoA/AoD) associated with the NLOS component, and $\boldsymbol{b}_{IRS}(.)$represents the array response vector at the IRS. Note that $\boldsymbol{R}_{IR}^{NLoS}$and $\boldsymbol{G}_{TI}^{NLoS}$represent the Rayleigh fading components, for channel $\boldsymbol{R}$ and $\boldsymbol{G}$, respectively, leading to the deterministic *LoS* channel when $v \to \infty$, and the Rayleigh fading

DOI: 10.31695/IJASRE.2022.8.10.1

channel when ν = 0. In addition, each of the above large scale fading parameters, ξ, can be described via a linear model as expressed below:

$$\xi = a + 10b\log_{10}(d) + \varsigma \tag{20}$$

in which d denotes the link distance, and $\varsigma \sim \mathrm{NC}(0,\sigma^2)$ is lognormal term accounting for variances.

4. PERFORMANCE OF IRS-ASSISTED OAM-MIMO COMMUNICATION WITH PASR SCHEME

4.1 Orthogonality Verification

An EM wave with a helical phase front *exp(iφl)* carries an OAM-mode related to *l*, where *φ* is the azimuthal angle and *l* is an unbounded number (referred as the order of OAM-mode). The phase front of an OAM-mode twists along the propagation direction. According to the Nyquist theorem, an upper limit on the largest OAM mode *l* that can be resolved, namely, $|l|<N/2$.

Algorithm 1: IRS-assisted OAM-MIMO communication with PASR scheme	
	Input: ***G, H*** *and* ***R,*** *N, M, K, S, d,* d_1, R_t, R_r, *B, SNR*
	Output: C_{OAM}^{IRS}
1	Initialize. *k =1, m =1, i =1,*
2	**Generate** $\boldsymbol{\theta}$ (any random phase shift) and find $\boldsymbol{\Theta}$ according to (8);
3	***For m=1:M***
4	***For*** l_i***=1:*** l_N
5	**Evaluate** $\boldsymbol{F}_T$ and $\boldsymbol{W}_R$ according to Eq. (7) and Eq. (10), respectively;
6	**Evaluate** $\boldsymbol{H}_{OAM}^{PASR}(l_i)$ according to Eq. (9) and (11); $i = i + 1$;
7	**end**
8	**Obtain** C_{OAM}^{IRS} by solving Eq. (23), $m = m + 1$;
9	**end**
10	Obtain the capacity for IRS-assisted OAM-MIMO communication with PASR

Therefore, the above restrict condition should also be considered in the PASR scheme without exception while having a deformed definition as $|l|<\mu N/2$. It is apparent that any two sampled OAM waves with modes l_{n1} and l_{n2} will remain orthogonal when:

$$mod\left(\left|l_{n1}-l_{n2}\right|,\mu\right)=0 \tag{21}$$

$$mod\left(\left|l_{n1}-l_{n2}\right|,\mu M\right)\neq 0 \tag{22}$$

Although the orthogonality of different OAM modes is a little damaged and there are some other crosstalk OAM modes, the main transmission OAM modes can be kept and distinguished by introducing some specific digital signal processing methods.

4.2 Capacity Analysis

To gain more explicit insights into the impact of partial aperture sampling receiving (PASR) scheme on the system performance, we now consider the simplified setting illustrated in Fig.1. When both the transmitter and the receiver know the channel state information (CSI), the channel capacity for IRS-assisted system with PASR is derived as:

$$C_{OAM\text{-}PASR}^{IRS}=\sum_{i=1}^{L}B\log_2\left(1+\frac{P}{N}SINR_i^{PASR}\right) \tag{23}$$

where

$$SINR_i^{PASR}=\frac{\left|h_{i,i}^{PASR}\right|^2}{\sum_{j\neq i}\left|h_{i,j}^{PASR}\right|^2+\sigma_i^2} \tag{24}$$

where $h_{i,i}^{PASR}$ is the OAM channel transmission gain for the channel matrix of the IRS-assisted OAM-MIMO communication with PASR corresponding to l_i-OAM mode and $h_{i,j}^{PASR}(i\neq j)$ indicates the mode migration of the l_i-mode OAM channel to channels of

DOI: 10.31695/IJASRE.2022.8.10.1

other modes. In addition $P_i = P/L$ represents the transmit power corresponding to the l_i-OAM mode, the notation B is the Bandwidth and σ_i^2 is the receiver noise variance. In addition, the IRS-Assisted OAMMIMO Communication with PASR scheme is given by Algorithm 1. Note that the channel capacity of IRS-Assisted OAMMIMO Communication (without PASR scheme) will consider the whole receiving scheme that collects the fields within the angular aperture from 0 to 2π.

5. NUMERICAL RESULTS AND ANALYSIS

In this section, we provide the numerical results that (i) validate the derived channel capacity for IRS-assisted OAM-MIMO Communication With/out PASR, provide (ii) insights on the angular aperture needed for efficient (de)-multiplex OAM modes, and (iii) insights for the performance limit of IRS-assisted OAM-MIMO Communication over propagation distance.

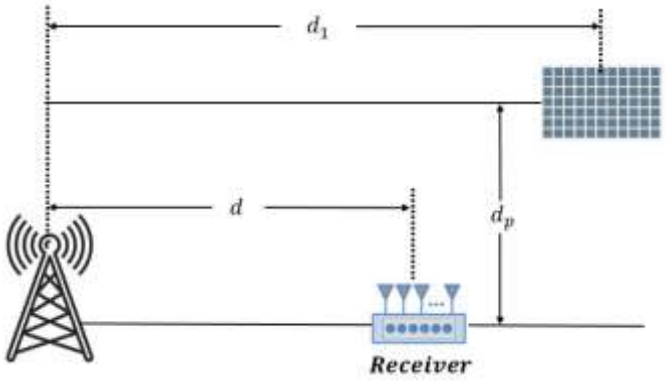

Figure 3. Simulation setup of the transmitter, IRS, and receiver

In our simulations, we consider a scenario shown in Figure 3, where the IRS is deployed in a position that has line of sight is respectively calculated as:

$$d_{TI} = \sqrt{d^2 + d_p^2} \tag{25}$$

$$d_{IR} = \sqrt{\left(d_1 - d\right)^2 + d_p^2} \tag{26}$$

where d is the distance from the transmitter and receiver, d_p is the vertical distance from two lines and d_1 is the horizontal distance from the transmitter and IRS. The other default simulation parameters are summarized in Table 1.

Table 1. Simulation parameters, symbols and their values

Parameters	symbols	values
The wavelength	λ	0.01
Vertical distance between two lines	d_p	2
Horizontal distance between Tx - IRS	d_1	30
Horizontal distance between Tx - Receiver	d	15
Signal to Noise Ratio	SNR	30 dB
Radius of transmit and receive antenna array	R_t, R_r	0.5λ
The mode set generated	L	{-6, -2, +2, +6}
Number of transmitting/receiving antenna elements	N, M	4
Bandwidth	B	20MHz
Number of elements at IRS	K	4
The circular arc	1/μ	1/4
The Rician k-factor	υ	5 dB

Figure 4. (a) Compares the capacities of conventional OAM based MIMO communication system and that of IRS assisted OAM-MIMO communication system concerning *SINR* by considering different antenna configurations. In the case of 16×16, the capacities for both systems increase with the increasing *SINR*. Moreover, the performance of the IRS assisted OAM-MIMO communication system is greater than that of OAM-MIMO communication system. When the antenna configuration is 4×4, the curve of capacity over *SINR* keeps a positive slope.

DOI: 10.31695/IJASRE.2022.8.10.1

In figure 4 (b), we present the capacities of OAM-MIMO Communication and IRS assisted OAM-MIMO Communication versus SINR by varying the transmission distance d_{TR} between transmit and receive UCAs. In our analysis, 4×4 configuration is considered and D_0 is fixed. It can be shown that the capacities for both systems increase with the increasing of SINR. Moreover, the capacities decrease with the increasing transmission distance. We can observe that the performance of IRS assisted OAM-MIMO Communication is better than that of OAM-MIMO Communication.

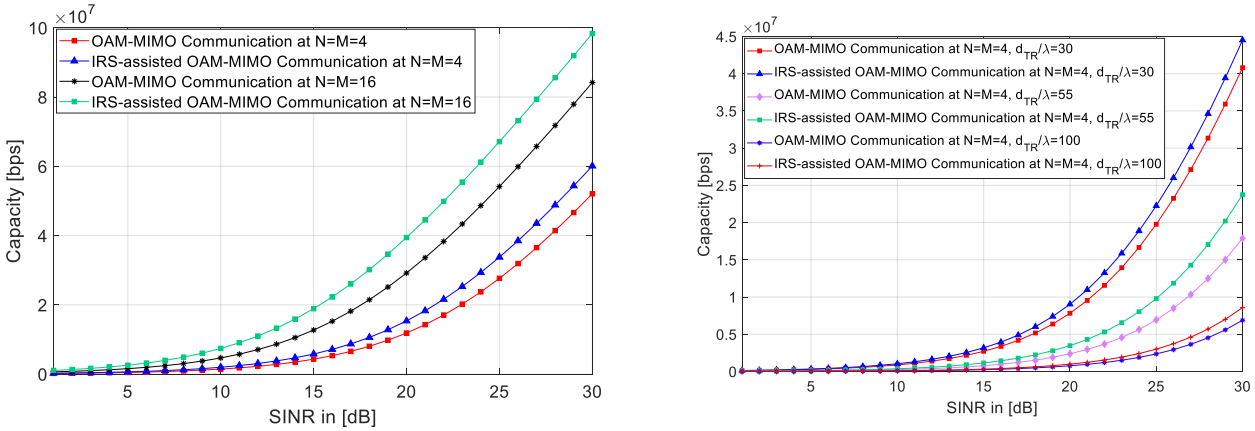

Figure 4. (a) Capacity of OAM-MIMO Communication with/out IRS at different values of N, (b) capacities of OAM-MIMO Communication and IRS assisted OAM-MIMO Communication versus the transmission distance.

In Figure 5, the channel capacity of an IRS-supported OAM-MIMO communication system using the PASR scheme is shown via the influence of SINR. To ensure the compact size and ease of implementation at the receiving end, we consider using four antenna elements evenly arranged on a partial arc to sample the four overlapping OAM waves. It can be seen that for efficient demultiplexing of the four OAM modes, only $\pi/2$ angular arc is needed. In addition, the achievable capacity of the IRS assisted system with PASR scheme is larger than that of IRS-assisted system without PASR scheme, and then increases gradually as the SNR increases.

Figure 6 reveals the capacity versus SINR for the IRS assisted OAM-MIMO communication system with/without PASR scheme over different values of Rician factor (i.e. υ) when $d_1 = 30\lambda$, $d_p = 2\lambda$ and$d = 15\lambda$, when the antenna configuration is 4×4. As can be readily observed, the capacity for both cases increases when the Rician factor v increases. When $\upsilon > 1$, the capacities of the IRS assisted OAM-MIMO communication system with/without PASR scheme is slightly increased. Since most of the power is transmitted along with the LoS path, higher capacity transmission is achieved, and when υ tending to positive infinity, the capacities will still increasing and tends to be equal to the capacity of the IRS-assisted OAM-MIMO communication with/without PASR scheme over the LoS channel. These results prove again that the proposed system with PASR scheme still has an excellent performance as compared to the system without PASR scheme.

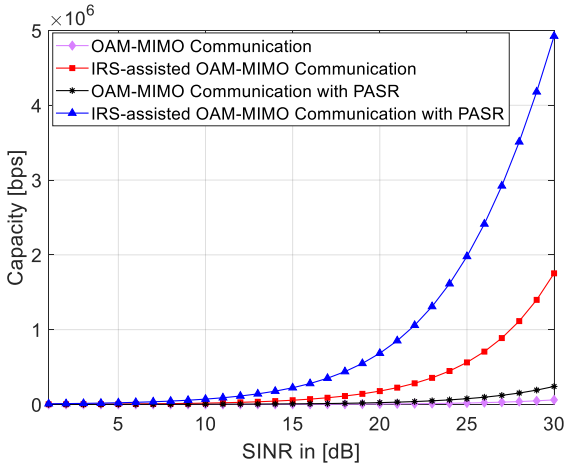

Figure 5 Capacity of IRS aided OAM-MIMO Communication with/out PASR scheme

DOI: 10.31695/IJASRE.2022.8.10.1

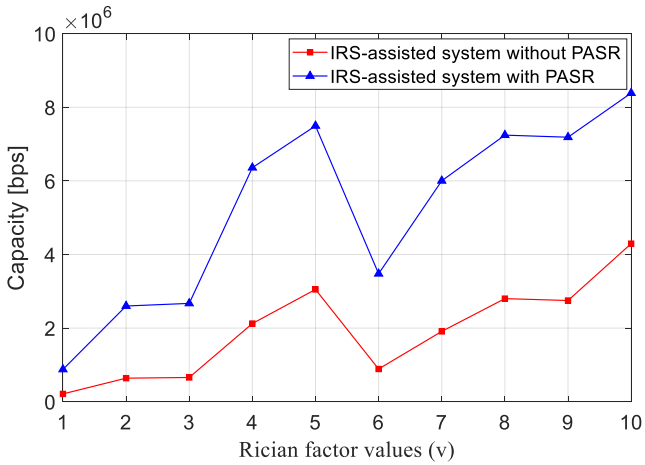

Figure 6 Capacity of the IRS aided OAM-MIMO communication system with/without PASR

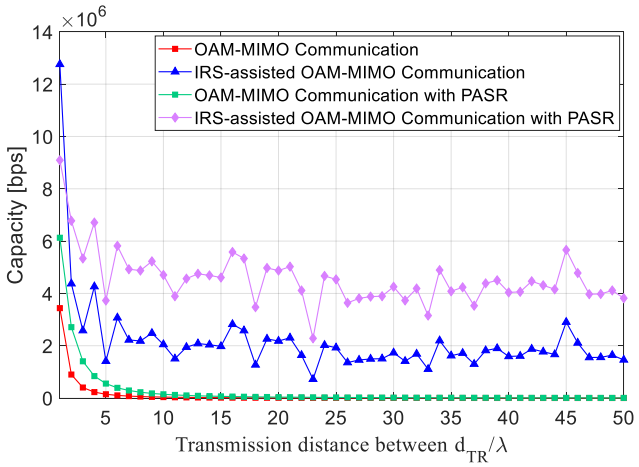

Figure 7 Capacity of IRS assisted OAM-MIMO Communication with/out PASR versus transmission distance

Figure 7 shows the channel capacities of the OAM-MIMO communication and IRS assisted OAM-MIMO communication system with/without PASR scheme when considering transmission distance by considering $d_1 = 30\lambda$ and $d_p = 2\lambda$. As can be readily observed, all the capacities decrease with increasing transmission distance. However, the IRS assisted OAM-MIMO communication system with PASR scheme obtains a better performance in a long distance transmission compared with the IRS assisted OAM-MIMO communication system due to the performance degradation over long transmission distance.

6. CONCLUSION

Intelligent Reflecting Surface (IRS)-assisted OAM wireless communication provides an effective solution for 5G or future wireless communications, especially if the link between transmitter and receiver is unfavorable. This paper considered a new method using Intelligent Reflecting Surface (IRS) to support OAM-based MIMO communication with PASR. We propose the system and channel models to characterize the IRS-assisted OAM-MIMO communication with PASR over the Rayleigh and Rician fading channels. We extended the work done in [22], by introducing a partial aperture sampling receiving (PASR) scheme to solve the larger aperture problem while still maintaining orthogonality in OAM radio communication system. From the numerical results we conclude that the IRS assisted OAM-MIMO communication system with PASR scheme performs better than the IRS-assisted system without PASR scheme in terms of channel capacity. In addition, IRS assisted OAM-MIMO communication system with PASR which uses only $\pi/2$ angular arc for efficient demultiplex of OAM modes provides greater performance than other cases considered. Finally, channel estimation scheme, hybrid beamforming or pre-coding scheme for IRS-assisted OAM-MIMO communication systems are reserved for future research for channel capacity maximization.

REFERENCES

[1] Shubair, S. Elmeadawy and R. M, "6G Wireless Communications: Future Technologies and Research Challenges," in *International Conference on Electrical and Computing Technologies and Applications (ICECTA)*, United Arab Emirates, 2019.

[2] Kim, Sungkyung, Jee-Hyeon Na, and Dong-Seung Kwon, "Network capacity and reliable transmission in ultra-dense networks sharing multiple carriers," *International Conference on Information and Communication Technology Convergence*

DOI: 10.31695/IJASRE.2022.8.10.1

(ICTC),, pp. 1149-1154, 2015.

[3] T. Marzetta, "Noncooperative cellular wireless with unlimited numbers of base station antennas," *EEE Trans. Wirel. Commun*, vol. 9, no. 11, p. 3590–3600, 2010.

[4] A. N. Uwaechia, N. M. Mahyuddin, M. F. Ain, N. M. A. Latiff and N. F.Za'bah, " On the Spectral-Efficiency of Low-Complexity and Resolution Hybrid Precoding and Combining Transceivers for mmWave MIMO Systems," *IEEE Access*, vol. 7, pp. 109259 - 109277, 2019.

[5] A. Singal, D. Kedia, N. Jaglan and S. D. Gupta. Singal, "Performance analysis of MIMO-OFDM system with transceiver hardware impairments," in *in 4th International Conference on Signal Processing, Computing and Control (ISPCC)*, Solan, India, 2017.

[6] S. Buzzi, T. E. Klein, H. V. Poor, C. Yang and A. Zappone, "A Survey of Energy-Efficient Techniques for 5G Networks and Challenges Ahead," *IEEE Journal on Selected Areas in Communications*, vol. 34, no. 4, pp. 697 - 709, 2016.

[7] Pinho, M. Ferreira and P, "Propagation at mmWaves frequencies: some considerations," in *in Telecoms Conference (ConfTELE)*, Leiria, Portugal, May 2021.

[8] R. Chen, H. Zhou, W.-X. Long and M. Moretti, "Spectral and energy efficiency of line-of-sight OAM-MIMO communication systems," *China Communications*, vol. 17, no. 9, pp. 119 - 127, 2020.

[9] R. Lyu, W. Cheng, W. Zhang and H. Zhang, " High Reliable Orbital Angular Momentum Wireless Communications for Space Information Networks," in *in 11th International Conference on Wireless Communications and Signal Processing (WCSP)*, Xi'an, China, 2019.

[10] T. Hu, Y. Wang and Q. Song, "Degrees of Freedom of UCA-Based Mode Division Multiplexing MIMO Systems," in *in 13th European Conference on Antennas and Propagation (EuCAP)*, Krakow, Poland, April 2019.

[11] H. Jing, W. Cheng, X.-G. Xia and H. Zhang, "Orbital-Angular- Momentum Versus MIMO: Orthogonality, Degree of Freedom, and Capacity," in *in IEEE 29th Annual International Symposium on Personal, Indoor and Mobile Radio Communications (PIMRC)*, Bologna, Italy, 2018.

[12] Zhu, Q., Jiang, T., Qu, D., Chen, D. and Zhou, N, " Radio vortex–multiple-input multiple-output communication systems with high capacity.," *IEEE Access*, vol. 3, pp. 2456-2464, 2015.

[13] D. Lee, H. Sasaki, H. Fukumoto, Y. Yagi, T. Kaho, H. Shiba and Takashi, "An Experimental Demonstration of 28 GHz Band Wireless OAMMIMO (Orbital Angular Momentum Multi-Input and Multi-Output) Multiplexing," in *in IEEE 87th Vehicular Technology Conference (VTC Spring)*, Porto, Portugal, June 2018.

[14] H. Wu, Y. Yuan, Z. Zhang and J. Cang, " UCA-based orbital angular momentum radio beam generation and reception under different array configurations," in *in Sixth International Conference on Wireless Communications and Signal Processing (WCSP)*, Hefei, China, 2014.

[15] G. Gradoni, T. M. Antonsen and E. Ott, " Influence of multi-path fading on MIMO/OAM communications," in *in International Conference on Electromagnetics in Advanced Applications (ICEAA)*, Granada, Spain, 2019.

[16] Zhang, Y. Zhao and C, "Compound Angular Lens for Radio Orbital Angular Momentum Coaxial Separation and Convergence," *IEEE Antennas and Wireless Propagation Letters,*, vol. 18, no. 10, pp. 2160 - 2164, Oct. 2019.

[17] Zhang, Y. Zhao and C, " Distributed Antennas Scheme for Orbital Angular Momentum Long-Distance Transmission," *IEEE Antennas and Wireless Propagation Letters*, vol. 19, no. 2, pp. 332 - 336, 2019.

[18] W. Zhang, S. Zheng, Y. Chen, X. Jin, H. Chi and X. Zhang, "Orbital Angular Momentum-Based Communications With Partial Arc Sampling Receiving," *IEEE Communications Letters*, vol. 20, no. 7, pp. 1381 -1384, 2016.

[19] Zhao, Q. Ma and H.-K, " Radio Vortex Communication System Using Partial Angular Aperture Receiving Scheme Under Atmospheric Turbulence," *IEEE Access*, vol. 8, pp. 152276 - 152285, 2020.

DOI: 10.31695/IJASRE.2022.8.10.1

[20] Y. Hu, S. Zheng, Z. Zhang, H. Chi, X. Jin and X. Zhang, " Simulation of orbital angular momentum radio communication systems based on partial aperture sampling receiving scheme," *IET Microwaves, Antennas and Propagation*, vol. 10, no. 10, p. 1043 – 1047, 2016.

[21] Y. Li, M. Jiang and G. Zhang, "Achievable Rate Maximization for Intelligent Reflecting Surface-Assisted Orbital Angular Momentum-Based Communication Systems," *IEEE Transactions on Vehicular Technology*, vol. 70, no. 7, pp. 7277 - 7282, 2021.

[22] Y. Wang, N. Cyprien, T. Hu and X. Liao, " IRS Aided OAM-MIMO Communication," in *in 2021 International Symposium on Antennas and Propagation (ISAP)* , Taipei, Taiwan, 2021.

[23] R. Chen, H. Zhou, M. Moretti, X. Wang and J. Li, " Orbital Angular Momentum Waves: Generation, Detection, and Emerging Applications," *IEEE Communications Surveys and Tutorials*, vol. 22, no. 2, pp. 840 - 868, November 2019.

[24] Pan, Cunhua; Ren, Hong; Wang, Kezhi; Xu, Wei; Elkashlan, Maged; Nallanathan, Arumugam, "Multicell MIMO Communications Relying on Intelligent Reflecting Surfaces," *IEEE Trans. Wirel. Commun.*, vol. 19, no. 8, p. 5218–5233, 2020.

[25] D.-W. Yue, H. H. Nguyen and Y. Sun, "mmWave Doubly-Massive- MIMO Communications Enhanced With an Intelligent Reflecting Surface: Asymptotic Analysis," *IEEE Access* , vol. 8, pp. 183774 - 183786, October 2020.

BIBRIOGRAPHY

NDAGIJIMANA Cyprien received the B.Sc in Engineering - Electronics and Telecommunication Engineering from the University of Rwanda-College of Science and Technology (UR-CST) in 2016. He got M.Sc. degree in Information and Communication Engineering with the Chongqing University of Posts and Telecommunications in 2022. His research interests lie in the field of Wireless Communication, specifically, the intelligent reflecting surfaces (IRS) assisted multiple-input multiple-output (MIMO), and orbital angular momentum (OAM) based wireless communication, MmWave communications and Terahertz communications.
Email: cyprienndagijimana@gmail.com

YANG WANG (Member, IEEE) received the M.S. and Ph.D. degrees from The University of Sheffield, U.K., in 2011 and 2015, respectively. He joined the School of Communications and Information Engineering, Chongqing University of Posts and Telecommunications (CQUPT), in 2015. He is currently an Associate Professor with the Communication Department, CQUPT. His research interests include antennas and propagation, radar signature management, phase-modulating microwave structures, and wireless communications.
Email: wangyang@cqupt.edu.cn

HAILAY TEKLEHAIMANOT received a M.Sc. degree in Information and Communication Engineering with the Chongqing University of Posts and Telecommunications in 2022. He is currently pursuing the PhD degree in Information and Communication Engineering with the Chongqing University of Posts and Telecommunications, Chongqing, China. His research interests include free-space optical (FSO) communication system and wireless Communication.
Email: L201920007@stu.cqupt.edu.cn

Olivier Hungurimana got M.Sc. degree in Embedded and Mobile System, specializing in Embedded System at Nelson Mandela African Institution of Sciences and Technology. He has a background in Electronics and Telecommunications Engineering obtained at University of Rwanda-College of science and technology in Kigali Rwanda. His interest lies in Information Communication and Technology of development in small scale industries sector and internet of things.
Email: olivierh@nm-aist.ac.tz

DOI: 10.31695/IJASRE.2022.8.10.1